AGU100 ADVANCING EARTH AND SPACE SCIENCE

Geophysical Research Letters

RESEARCH LETTER
10.1029/2018GL080812

Key Points:
- We examine dynamic source effects on along-dip rupture propagation for a Cascadia megathrust earthquake
- Simulated earthquake rupture is able to penetrate through the transition zone and reach the deeper slow-slip region
- Our results underscore the potential for a deeper downdip rupture and faster rupture speed than previously assumed in kinematic models

Supporting Information:
- Supporting Information S1

Correspondence to:
M. D. Ramos,
ramosmd@umich.edu

Citation:
Ramos, M. D., & Huang, Y. (2019). How the transition region along the Cascadia megathrust influences coseismic behavior: Insights from 2-D dynamic rupture simulations. *Geophysical Research Letters*, *46*, 1973–1983. https://doi.org/10.1029/2018GL080812

Received 7 OCT 2018
Accepted 30 JAN 2019
Accepted article online 4 FEB 2019
Published online 15 FEB 2019

©2019. American Geophysical Union. All Rights Reserved.

How the Transition Region Along the Cascadia Megathrust Influences Coseismic Behavior: Insights From 2-D Dynamic Rupture Simulations

Marlon D. Ramos[1] and Yihe Huang[1]

[1]Department of Earth and Environmental Sciences, University of Michigan, Ann Arbor, MI

Abstract There is a strong need to model potential rupture behaviors for the next Cascadia megathrust earthquake. However, there exists significant uncertainty regarding the extent of downdip rupture and rupture speed. To address this problem, we study how the transition region (i.e., the gap), which separates the locked from slow-slip regions, influences coseismic rupture propagation using 2-D dynamic rupture simulations governed by a slip-weakening friction law. We show that rupture propagation through the gap is strongly controlled by the amount of accumulated tectonic initial shear stress and gap friction level. A large amplitude negative dynamic stress drop is needed to arrest downdip rupture. We also observe downdip supershear rupture when the gradient in effective normal stress from the locked to slow-slip regions is dramatic. Our results justify kinematic rupture models that extend below the gap and suggests the possibility of high-frequency energy radiation during the next Cascadia megathrust earthquake.

Plain Language Summary How large, deep, and damaging a future earthquake will be depends on factors such as energy release that must be constrained by precise observations of previous earthquakes in the same area. But such data are rarely available. Instead, computer models of earthquakes guided by the laws of physics can provide us with estimates of potential ground shaking for a future event. In our study, we design two-dimensional earthquake simulations for the Cascadia fault below the northwestern United States coast and test different hypotheses for how stress may be accumulating at depth along this fault. Our models focus on a portion of the fault referred to as the "gap." The gap physically separates a shallow region that slips during large earthquakes from a deeper region that experiences intermittent slip between large earthquakes. A gap region similar to that in Cascadia is also found in Japan, Mexico, and around other active faults worldwide. We find that our simulated rupture is able to extend to deeper regions at faster speeds given the current understanding of stress levels and earthquake fault friction in the gap. While this work represents only a first step toward understanding how stresses and friction influence how the Cascadia fault might slip, it lays the foundation for modeling more complex physics that can help scientists better predict shaking from seismic waves.

1. Introduction

Anticipating potential rupture behaviors during the next great earthquake from the Cascadia subduction zone (CSZ) is of paramount importance to the northwestern United States coast (K. Wang & Tréhu, 2016). Paleoseismic studies have uncovered the potential of the CSZ to generate magnitude ~9 earthquakes through the mapping and dating of abruptly submerged coastal sediments (Atwater, 1987; Kelsey et al., 2002), characterization of marine turbidite deposits (Goldfinger et al., 2012, 2017), and paleo-tsunami records and modeling (Satake et al., 1996). Together these observations document repeated episodes of coseismic subsidence and tsunamigenesis. Models of the 1700 CE CSZ megathrust earthquake show temporal (Goldfinger et al., 2003; Priest et al., 2010) and spatial (Leonard et al., 2010; P. L. Wang et al., 2013) rupture variability along-strike, but the extent and characteristics of downdip rupture remains largely unknown. An outstanding question is if episodic tremor and slow-slip (ETS) events can be used as a proxy to map downdip rupture limits along subduction zone megathrusts. In Nankai, it has been observed that longer duration slow-slip events have, over time, occurred along a transition region that separates the locked from ETS regions of the megathrust (Kobayashi, 2012). Similar to Nankai, ETS in northern Cascadia is spatially distinct from the locked region and occurs at depths between 30 and 50 km (Gomberg, 2010; Rogers &

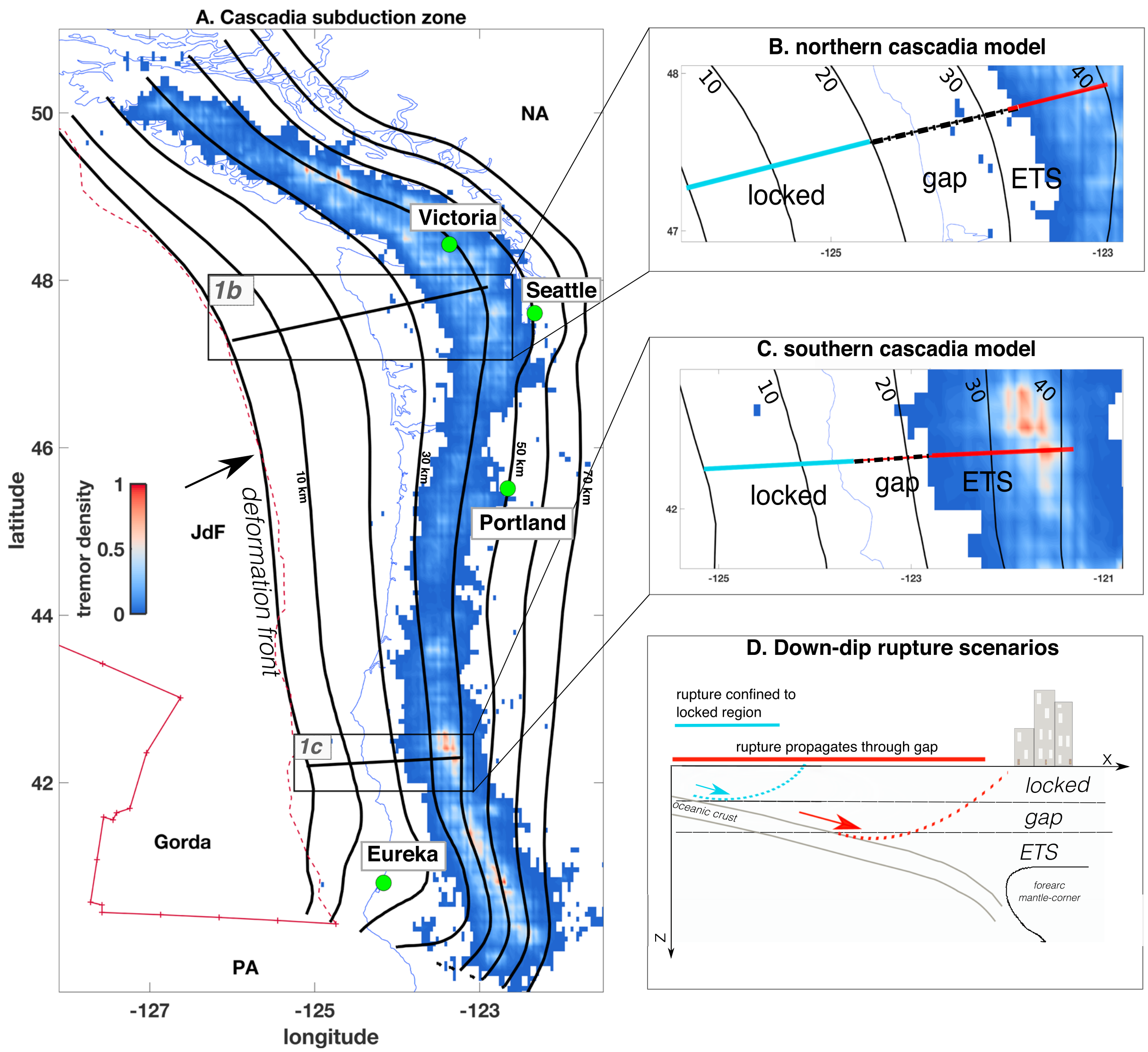

Figure 1. The Cascadia subduction zone. (a) Map of nonvolcanic tremor (normalized) density along the Cascadia megathrust from 2009 to 2018 (Wech & Creager, 2011). Plate interface depths are given by the bold black lines in 10 km intervals (McCrory et al., 2012). Plates are denoted as NA, PA, JdF, and Gorda from Bird (2003). (b) 2-D rupture model setup across northern Cascadia showing the locked (solid teal line), gap (dashed black line), and ETS (solid red line) megathrust regions. (c) 2-D rupture model setup across southern Cascadia. (d) Schematic drawing of the two downdip rupture scenarios that highlight how if rupture can penetrate into the gap, seismic waves are brought closer to populated areas, extending the length of the earthquake source model. ETS = episodic tremor and slow-slip; NA = North America; PA = Pacific; JdF = Juan de Fuca.

Dragert, 2003; Wech & Creager, 2011; Figure 1), but the frictional behavior and stress state within the transition region (i.e., the gap) for the CSZ is poorly constrained. Developing coseismic rupture models that explore the gamut of fault stress, rheology, and friction levels in the gap is critical to seismic hazards analysis because this region could exert strong control on downdip rupture propagation.

Kinematic rupture models show that ground motions from the Cascadia megathrust earthquake are significantly impacted by the choice of hypocentral depth, downdip rupture limit, rupture speed, slip distribution, and high-stress drop subevents (Delorey et al., 2014; Frankel et al., 2018; Melgar et al., 2016; Olsen et al., 2008; Wirth et al., 2018). In particular, Wirth et al. (2018) find that a deeper downdip rupture limit generally produces higher ground motion intensity for inland locations, mostly due to the deeper locations of high-stress drop (~20 MPa) subevents. It is also common to assume a range of 2–3 km/s for rupture speeds in kinematic rupture simulations. However, faster rupture usually results in larger ground motions (e.g., Graves et al., 2008), and an increase in the average rupture velocity from 2.1 to 2.3 km/s can lead to a factor of

1.5 difference in spectral acceleration values in Cascadia kinematic rupture models (Wirth et al., 2018). Our goal is thus to provide physically informed constraints on kinematic rupture properties for a future CSZ megathrust earthquake by considering rupture dynamics and our current understanding of stresses and fault friction.

A notable feature of the CSZ is its relative lack of seismicity near the plate interface (McCrory et al., 2012; Stone et al., 2018; Williams et al., 2011), which precludes conventional estimates of earthquake stress release (Scholz & Campos, 2012). However, recent insight into the state of shear stress based on the joint inversion of horizontal GPS and vertical tide-gauge data (Bruhat & Segall, 2016, 2017) suggests an abrupt gradient near the inferred downdip limit of the locked zone in northern Cascadia. In fact, negative shear stress rates in the gap appear to be a necessary condition to fit the vertical geodetic data, irrespective of imposed locking depth (Bruhat & Segall, 2016). We aim to test this particular shear stress profile in the gap below northern Cascadia while addressing uncertainties in its amplitude across the gap using 2-D dynamic earthquake rupture simulations operating under a linear slip-weakening friction law. We find that shear stress and friction levels in the gap play a principal role in governing downdip rupture propagation. In addition, we also design simulations to represent dynamically what may occur for a rougher and hydrated megathrust fault below southern Cascadia. Our simulations predict that rupture can break through the gap and propagate into the ETS region, unless the gap has large negative stress drops whose amplitudes exceed those predicted by geodetically derived shear stress rates. These results support a seismic hazard source model that extends below the locked region, which can be directly implemented in current kinematic rupture models (Frankel et al., 2018; Wirth et al., 2018). These 2-D dynamic rupture models can also be used to inform future 3-D CSZ dynamic rupture models and other megathrust faults that possess a separation between the locked and ETS regions (e.g., Nankai, Mexico; Brudzinski et al., 2016; Takagi et al., 2016).

2. Methodology

2.1. Model Geometry and Friction Law

We model the northern Cascadia megathrust as a 240-km-wide low-angle thrust fault dipping at ~11° that extends to a depth of 40 km (Figure 1b). Our along-dip model geometry is simplified because we want to emphasize dynamic effects from heterogeneous stress or friction conditions on rupture propagation. We consider only the upper 40 km because this depth extent adequately captures all three regions of interest along the megathrust: the locked, gap, and ETS zones. Similarly, the model geometry for southern Cascadia also extends to 40 km depth, but is only 160 km wide to reflect the steeper subduction angle (Figure 1c; McCrory et al., 2012). Both faults are embedded in a homogeneous, isotropic, and linearly elastic half-space characterized by a shear modulus (G) of 30.0 GPa and Poisson's ratio (υ) of 0.25. A hemispherical absorbing boundary encloses the lower half of each computational domain. Dynamic rupture propagation is solved using the 2-D spectral element code SEM2DPACK (Ampuero, 2009).

We treat earthquake rupture as a propagating shear crack operating under linear slip-weakening friction. This minimalistic model allows us to focus on the dynamic contribution of fault stresses to along-dip rupture propagation. A further analysis of more complex friction laws such as rate-and-state (e.g., Dieterich, 1979; Rice et al., 2001), flash heating (e.g., Goldsby & Tullis, 2011), and thermal pressurization (e.g., Bizzarri & Cocco, 2006) will provide more insights into the rupture propagation style (e.g., crack-like vs pulse-like rupture) and the influence of fluids and temperature, but first-order rupture characteristics such as downdip rupture extent can be captured by the dynamic interaction of fault stresses and frictional strengths governed by the slip-weakening friction law. We select a critical-slip distance (D_c) of 2 m, static friction coefficient (μ_s) of 0.6, and dynamic friction coefficient (μ_d) of 0.2 along the fault,

$$\mu = \max\left[\mu_d, \mu_s - \frac{\mu_s - \mu_d}{D_c} D\right], \tag{1}$$

where D is slip (Ida, 1972). The static and dynamic fault shear strengths are defined as the product between the effective normal stress and the static and dynamic friction coefficients, respectively. In the linear slip-weakening friction law, slip occurs when initial shear stresses overcome the static shear strength of the fault, and shear stresses drop linearly to the dynamic shear strength when slip reaches D_c. The static and dynamic friction coefficients are chosen to be consistent with experiments conducted at high confining stress and at comparable coseismic slip-rates (i.e., Byerlee, 1978; Goldsby & Tullis, 2011). Our choice of 2 m agrees with D_c values used in previous slip-weakening simulations of the Tohoku-Oki earthquake, which constrain D_c using the frequency range of back-projection results (Huang et al., 2014).

2.2. Constraints on Cascadia Megathrust Stress Conditions

Pore pressure is inferred to be at or near lithostatic levels in proximity to the forearc-mantle corner (Audet et al., 2009; Liu & Rice, 2009; Wech & Creager, 2011). Higher pore pressure, which translates to lower effective normal stress levels, is also supported by ETS stress drop measurements that range between 0.01 and 1.0 MPa (Gao et al., 2012) and the fact that small stress perturbations on the order of ~0.01 MPa influence tremor activity (Nakata et al., 2008; Rubinstein et al., 2007). The effective normal stress within the ETS region is thus set to 1 MPa in each simulation for both Cascadia models. For northern Cascadia, effective normal stress in the locked region is set to a constant 50 MPa and tapers down to 10 MPa in the upper 5 km of the fault, consistent with other fault models for northern Cascadia (Li & Liu, 2016; Liu & Rice, 2009). For each simulation, we assume a decreasing linear gradient in stress across the gap region. Within the locked region in southern Cascadia, however, we select a lower effective normal stress level of 30 MPa to represent a higher state of hydration, which implies elevated pore pressures (Stone et al., 2018).

We estimate initial shear stress conditions for northern Cascadia using shear stress rate and gap width constraints below the Olympic Peninsula (Bruhat & Segall, 2016, 2017; Holtkamp & Brudzinski, 2010; Schmalzle et al., 2014). The Bruhat and Segall (2016) inversion analysis requires an abrupt transition in shear stress rate at the base of the locked zone, assuming creep is not present above the specified locking depth. They deduced an upper bound of 35 kPa/year near the bottom of the locked zone (~21 km depth), which we multiply by an average megathrust recurrence interval of ~505 years (Goldfinger et al., 2017) to arrive at the accumulated tectonic shear stress at the bottom of the locked zone (17.7 MPa) in our northern Cascadia models. By assuming a complete stress drop during the last megathrust rupture, we use the dynamic fault strength to represent the stress state immediately after the last megathrust earthquake. Thus, our initial shear stress level is the sum of the dynamic fault strength and the accumulated tectonic shear stress, which leads to an initial shear stress level of 27.7 MPa near the bottom of the locked zone (Figure 2). Applying the same procedure to the gap region, where a negative shear stress rate of −2.5 kPa/year is estimated (Bruhat & Segall, 2016), we calculate an initial shear stress level of ~4.3 MPa. Within the ETS region, we select a nominal initial shear stress level of 0.21 MPa to provide some positive stress drop. In some simulations, we increase the dynamic friction coefficient equal to or greater than the static friction coefficient value to represent a slip-neutral or slip-strengthening frictional behavior in the gap region. The accumulated tectonic shear stress is also added to the dynamic fault strength in these cases to obtain the initial shear stress levels.

We use a different approach to estimate shear stress levels in the locked region for southern Cascadia. Estimations of the in situ stress state near the Mendicino Triple Junction suggest effective friction coefficients between 0.1 and 0.2 (Li et al., 2018). Since the initial shear stresses calculated from these effective friction values are below our dynamic shear strength levels, we select a slightly larger effective friction coefficient (0.21) and multiply this value by the effective normal stress to obtain an average initial shear stress of 6.3 MPa in the locked region. Our model also accounts for a comparatively rougher megathrust fault as inferred from the highly deformed Gorda plate subducting below southern Cascadia (Gulick et al., 1998; McCrory et al., 2012) and the marked increase in seismicity rate here (Chen & McGuire, 2016; Li et al., 2018; Stone et al., 2018) by incorporating heterogeneous distributions of effective normal and initial shear stress (see supporting information).

In our simulations, the dynamic strength affects the fault strength excess (the difference between the static shear strength and initial shear stress), whereas the accumulated tectonic shear stress is equivalent to the dynamic stress drop (the difference between the initial shear stress and dynamic shear strength). We use the S-ratio to quantify the ratio between fault strength excess and dynamic stress drop to investigate how rupture velocity may transition to amplitudes exceeding the shear-wave velocity, a phenomenon termed supershear (Das & Aki, 1977; see supporting information). A lower but positive S-ratio implies a higher initial shear stress given the same frictional strengths. But a deficit in initial shear stress relative to

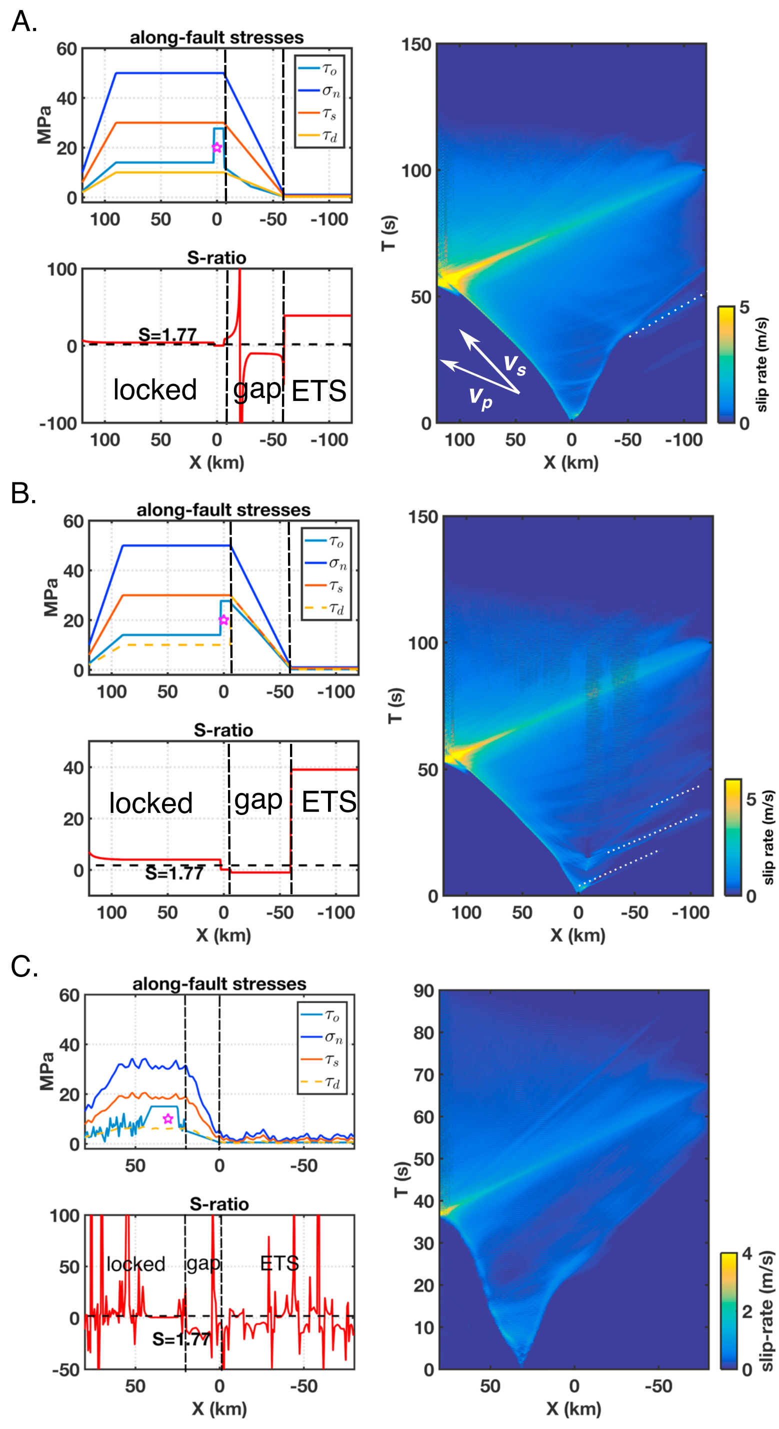

Figure 2. Dynamic rupture simulations for northern and southern Cascadia. The heavy dashed black lines partition the fault into the locked, gap, and ETS regions. Along-dip stresses, S-ratio, and resulting spatiotemporal rupture histories are shown for each model. Each fault stress distribution shows the initial shear stress (τ_o), effective normal stress (σ_n), static shear strength (τ_s), and dynamic shear strength (τ_d). The pink star indicates the hypocenter. Each S-ratio plot depicts the locked, gap, and ETS zones along the fault as well as a reference level of 1.77 for supershear (Andrews, 1976). (a) Northern Cascadia model assuming an initial shear stress asperity at the base of the locked region of the fault (Bruhat & Segall, 2016), a negative shear stress rate amplitude of −2.5 kPa/year in the gap, and the entire fault is assumed slip-weakening. (b) A northern Cascadia model assuming a dynamic friction coefficient level of 0.6 and an approximately −2.5 kPa/year shear stress rate in the gap. This model generates multiple downdip supershear daughter-cracks (white dotted lines). (c) Southern Cascadia model incorporating heterogeneous τ_o and σ_n perturbations to represent a rougher fault. ETS = episodic tremor and slow-slip.

dynamic fault strength, which corresponds to a negative S-ratio, typically hinders rupture propagation. For mode II cracks governed by slip-weakening friction in homogeneous 2-D media supershear is encouraged when the S-ratio is below 1.77 (Andrews, 1985; Dunham, 2007).

2.3. Hypocenter Locations and Nucleation Procedure

The northern Cascadia model hypocenter is set to the downdip limit of the locked megathrust at 20 km depth (Bruhat & Segall, 2016; Figures 2a and 2b). For the southern Cascadia model, we select a shallower hypocenter at 12 km depth, to be consistent with the downdip locking depth estimated there (Schmalzle et al., 2014; Figure 2c). We think these hypocenter choices are reasonable given (1) the maximum shear stress rate is located immediately above the gap from the Bruhat and Segall (2016) study and (2) the similar range of hypocenter depths of great earthquakes from global observations (Lay et al., 2012). Rupture is artificially nucleated in both Cascadia models using the time-weakening method (Andrews, 1985; see supporting information).

3. Results

3.1. Northern Cascadia Simulations

To thoroughly study controls on downdip rupture propagation, we conduct a wide range of rupture models for both northern and southern Cascadia, assuming different dynamic friction coefficients, initial shear stress rate values, and effective normal stress levels in the locked, gap, and ETS regions (Table S2 and Figures 3a and 3b). We highlight the results of three shear stress profiles across the gap in northern and southern Cascadia in Figure 2. In all three models, the initial shear stress asperity is at the base of the locked megathrust where rupture is nucleated. We simulate rupture until the rupture stops completely (150 or 90 s). The shallowest portion (depths <5 km) of the megathrust is assumed to be slip-weakening due to a lack of constraints, which leads to strong free-surface reflections (Nielsen, 1998).

Our first simulation considers the Bruhat and Segall (2016) stress rate profile from their preferred model and illustrates the effect of a negative dynamic stress drop in the gap (Figure 2a). Whereas this stress condition in the gap should represent a barrier to rupture propagation, downdip rupture arrest is not observed in this scenario. Rupture can penetrate through the gap because the dynamic stress drop at the base of the locked megathrust provides sufficient energy to drive rupture downdip, regardless if dynamic stress drop becomes abruptly negative in the gap. The downdip rupture front propagates at ~1 km/s in the gap and then accelerates to ~2.8 km/s when it encounters the low static shear strength ETS region. Note that a daughter-crack indicative of a supershear rupture transition also emerges in the ETS region (Figure 2a). In contrast, the updip rupture front is smooth and bifurcates at X = 90 km due to the tapering of stresses toward the deformation front (Figure 2a).

To explore what conditions could hinder downdip rupture propagation, we first assume slip-neutral friction across the gap (Figure 2b). This means that the dynamic friction coefficient in the gap region is equal to the static level, which does not favor crack growth. We observe, however, that rupture still manages to propagate downdip, although the slip-rate is on average lower compared to the first simulation (Figure 2b). We also observe several daughter-cracks with speeds exceeding the shear-wave velocity branching out from the primary downdip rupture front in the gap (Figure 2b). The updip rupture front is unaffected by slip-neutral gap friction.

We found that the negative shear stress rate in the gap predicted by the Bruhat and Segall (2016) model by itself is insufficient to arrest downdip rupture. Downdip rupture is impeded only if the gap has dynamic frictional levels greater than 0.6 and a negative shear stress rate of approximately −12 kPa/year is assumed in the gap, which leads to a much larger negative stress drop that inferred from the Bruhat and Segall (2016) model (Figures S1a and S2). We can also assume an even more negative dynamic stress drop of −25.1 kPa/year and slip-neutral friction to arrest downdip rupture as well (Figures S1b and S2). While downdip rupture propagation beyond the influence of the time-weakening nucleation procedure is subdued, it does not hinder the free-surface reflection as it propagates back down the fault. We found that one way to effectively dampen the free-surface reflection is to increase the dynamic friction coefficient to at least 0.54 in the upper 5 km of the megathrust (Figure S3). We also tested a model where slip-neutral friction is present only in the ETS region, but this model does not arrest downdip rupture and produces rupture features that

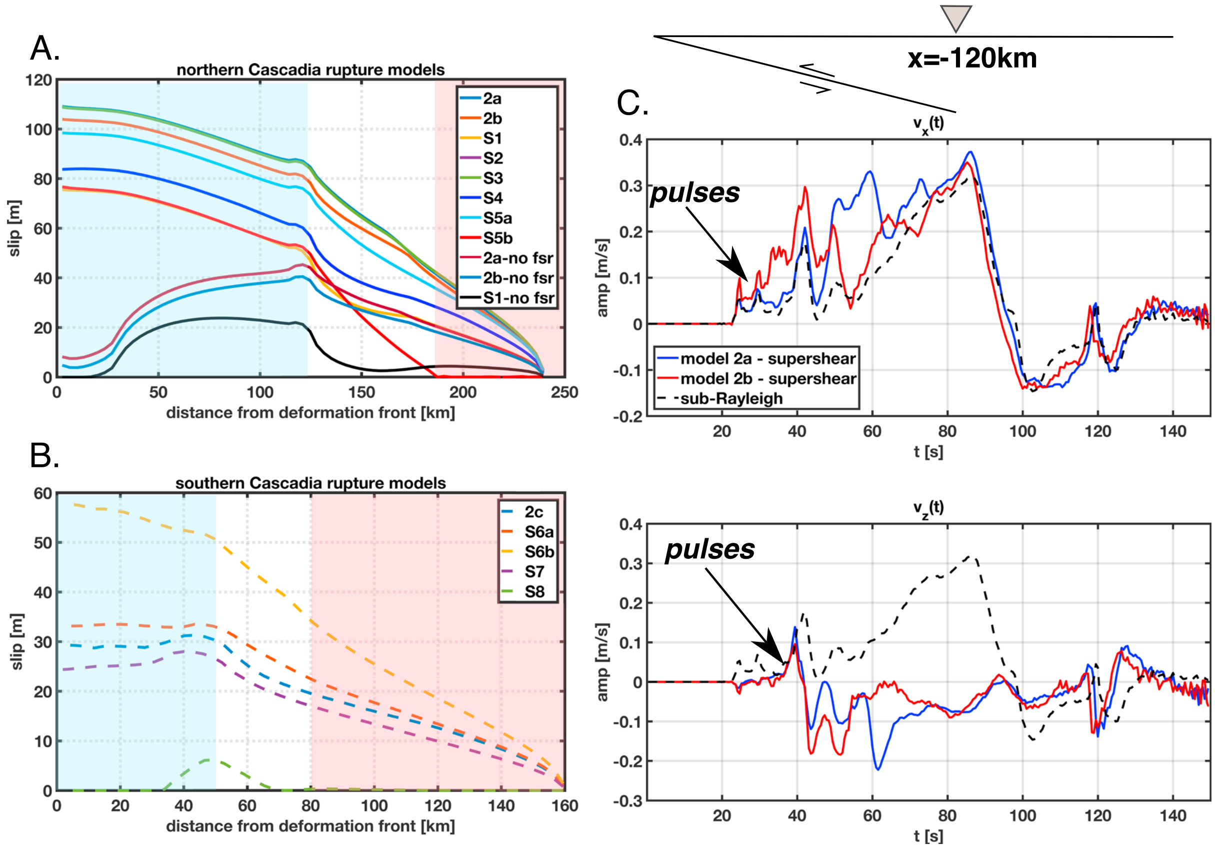

Figure 3. Final along-fault slip distributions for all rupture models and the effect of downdip supershear on synthetic waveforms. "No-fsr" models have the free-surface reflection suppressed by assuming slip-neutral friction in the upper 5 km of the fault. (a) Coseismic slip for northern Cascadia rupture models where the light blue and red regions signify the locked and ETS regions of the fault, respectively. The gap region is left unshaded. (b) Coseismic slip for southern Cascadia models. (c) Horizontal (top) and vertical (bottom) component seismograms for a station located at x = −120 km, immediately above the downdip edge of the modeled northern Cascadia megathrust. The wave pulses resulting from supershear rupture are indicated.

are qualitatively similar to the slip-weakening simulation (Figure S4). Assuming a lower initial shear stress rate at the base of the locked/gap regions and slip-weakening gap friction does not preclude downdip rupture either, but does retard the downdip rupture speed in the gap to less than 1 km/s (Figure S5). Our results show that it is the stresses and frictional conditions of the gap region, not the ETS region, that determine whether downdip rupture can penetrate deeper.

On the other hand, the observation of supershear rupture velocity near the ETS region strongly depends on the stresses and frictional conditions of the ETS region. If we depart from the 1 MPa effective normal stress level constraint in the ETS region, and either assume a lower fault strength gradient across the gap (e.g., Figure S6a) or a uniform fault strength level across the gap and ETS zones (e.g., Figure S6b), we instead observe a coherent downdip rupture front that propagates at sub-Rayleigh speeds. These results demonstrate the sensitivity of the downdip kinematic properties to both the gap and ETS regions.

We summarize the final slip profiles from all northern Cascadia rupture models in Figure 3a. Models that assume a higher static shear strength across the gap and ETS regions or slip-strengthening frictional behavior in the gap produce lower downdip slip amplitude (Figures 3a and S6b). However, a majority of the models produce significant slip (>60 m) in the locked region and considerable slip (~20 m on average) in the gap and ETS regions (Figure 3a). The peak slip in simulations with free-surface reflections occurs near the deformation front and is larger than that prescribed in previous kinematic rupture simulations. But the peak slip is more comparable to that prescribed in previous kinematic rupture simulations when free-surface effects are suppressed. Note that our slip profiles are more representative of the along-dip slip distribution through the hypocenter.

3.2. Southern Cascadia Simulation Results

The southern Cascadia region below 43°N latitude is characterized by a steeper subduction angle, greater seismicity, and ample sediment entering the subduction zone that most likely has greater volumes of entrained water compared to northern Cascadia (Flueh et al., 1998; Stone et al., 2018; Trehu et al., 1994). Since the spatial distribution of nonvolcanic tremor suggests a shorter gap width (Figure 2c), we model the gap as an ~20 km wide region across where both effective normal and initial shear stresses linearly decrease. We combine the effects of a rough fault and higher seismicity by implementing a stochastic effective normal stress and initial shear stress field, respectively (see supplementary information for details). Such highly heterogeneous effective normal and initial shear stress conditions lead to significant fluctuations in the S-ratio, but still downdip rupture is not arrested (Figure 2c). The shorter fault length of southern Cascadia megathrust leads to an overall shorter rupture duration compared to northern Cascadia rupture. We do not observe any daughter-cracks either updip or downdip. We also consider the effect of a rougher fault or higher seismicity separately (i.e., Figures S7a and S7b) and do not find that either stress parameterization produces drastically different results on the spatiotemporal rupture character; but a highly heterogeneous initial shear stress distribution along the locked region nearly doubles the final slip amplitude at the deformation front (Figure 3b). We acknowledge that either shear or normal stress distribution depends on the particular stochastic stress level along the fault. However, the conclusion of rupture penetration through the gap is unaffected by these different stress parameterizations.

We also investigate the effects of the gap width by reducing it to approximately 500 m. Despite the drastic and unlikely gradient in fault strength, it shows that supershear transition can be attained almost immediately after the time-weakening procedure ceases (Figure S8). In contrast to the northern Cascadia models, the southern Cascadia models do not require the dynamic friction to increase completely to the static level in order to arrest downdip rupture: Both updip and downdip rupture fronts are impeded by a dynamic friction greater than 0.3 in the gap (Figure S9). Overall, the average final slip of southern Cascadia rupture models is lower than that of northern Cascadia due to the smaller dynamic stress drop amplitudes in southern Cascadia (Figure 3b).

4. Discussion and Conclusion

We consider a model of shear stress accumulation that implies a strong contrast in dynamic stress drop (positive to negative) at the locked/gap interface below northern Cascadia based on the shear stress rate estimated by Bruhat and Segall (2016). However, they assumed that the depth distribution of interseismic slip-rate is time invariant. Bruhat and Segall (2017) allowed updip propagation of interseismic slip into the locked region in their quasi-dynamic models and showed a similar transition in shear stress rate from the locked to gap regions. Their stress rate estimates vary with different model parameters. Among all the best-fitting models, the largest negative stress rate in the gap is approximately −20 kPa/year, which is at the lower limit of the amplitude of negative shear stress rate that arrests downdip rupture in our models. For example, assuming the same dynamic shear strength level and slip-neutral friction in the simulations shown in Figures S1b and 2a, the more negative shear stress rate of approximately −25 kPa/year in Figure S1b simulation leads to lower initial shear stress level in the gap region than the Figure 2a simulation. This result demonstrates that the arrest of downdip rupture can be accomplished if the gap is slip-neutral, but with a negative shear stress rate that is an order of magnitude lower than the preferred Bruhat and Segall (2016) model.

Supershear rupture propagation can lead to increased ground velocities at greater distances (Andrews, 2010) and has been suggested by back-projection analysis of the Tohoku-Oki megathrust earthquake (Meng et al., 2011). Our simulations show that the downdip rupture front can produce supershear daughter-cracks when encountering the ETS region (e.g., Figures 2a and 2b and Table S2). An exceptionally low amplitude effective normal stress in the ETS region and a high amplitude initial shear stress asperity are necessary to allow supershear daughter-cracks to jump ahead of the main rupture front downdip. To isolate the supershear effect, we assume slip-neutral friction in the upper 5 km of the fault to suppress the free-surface reflection and compare supershear rupture models to a sub-Rayleigh rupture model where the effective normal stress in the ETS region is increased to 10 MPa. We observe multiple wave pulses resulting from the supershear rupture in velocity seismograms recorded by a station near the location of Seattle (Figure 3c). The pulses give rise to larger high-frequency ground motions in the first 40 s (~20–60 s). However, the peak ground velocity generated by the supershear ruptures are comparable to that generated by the sub-Rayleigh rupture. From a seismic hazard standpoint, the combined effects of an offshore hypocenter (i.e., directivity), a deeper downdip rupture limit, and a higher rupture velocity could couple to low-velocity sedimentary basin amplification (Frankel et al., 2018; Olsen et al., 2008; Wirth et al., 2018) and change current ground motion prediction equation estimates. Supershear rupture velocity is one kinematic parameter that should be incorporated in future kinematic rupture models.

Our model for southern Cascadia also shows rupture penetrating through the gap (Figures 2c, S6, and S7). Kinematic rupture models suggest that if rupture extends to the top of the ETS region, coseismic uplift is predicted using an elastic half-space (Wirth et al., 2018). Paleoseismic observations in the southern CSZ, on the other hand, support coseismic subsidence during the last megathrust rupture in 1700 CE (Leonard et al., 2010; P. L. Wang et al., 2013). While we also employed an elastic half-space model to simulate dynamic rupture, inelastic material effects around the fault zone and upper plate, or a nonplanar free-surface could also influence predicted coseismic uplift and subsidence signals (Tinti & Armigliato, 2002). Alternatively, the gap in southern Cascadia may behave as a barrier to downdip rupture relative to the ETS region if dynamic friction levels exceed 0.3 in the gap (i.e., Figure S6) or if viscous-shear effects can impact coseismic rupture (Gao & Wang, 2017). It is also unclear whether the next Cascadia earthquake will rupture in a similar way as the 1700 Cascadia earthquake (P. L. Wang et al., 2013; Wirth et al., 2018).

In addition to heterogeneous stresses or friction, slab geometry may significantly influence rupture propagation. Recent studies have suggested that smoother megathrusts naturally lead to larger earthquakes because a more homogeneous interface allows for more uniform fault strength distributions (Bletery et al., 2016). Since the incoming plate offshore northern Cascadia is smoother compared to southern Cascadia (van Rijsingen et al., 2018), along-strike rupture propagation may be easier to sustain and allow ~M9 ruptures to develop. For lack of direct updip constraints on the shear stress state across the CSZ, we did not rigorously explore the parameter space beyond increasing the dynamic friction to limit the free-surface reflection. Previous dynamic rupture models of the 2011 Tohoku-Oki earthquake show that the free-surface reflection and shallow subduction angle assisted near-trench slip (Huang et al., 2012, 2014), and we obtain a similar result in our 2-D models (Figures 3a and 3b). Given the shallow subduction angle in the upper 5 km depth for most of the CSZ (<8°), reflected waves in the wedge or deformation front may indeed form a viable mechanism to generate relatively large slip there, emphasizing the tsunami hazard (Lotto et al., 2018; Melgar et al., 2016).

Our dynamic rupture simulations show that if a sharp shear stress gradient exists at the base of the locked zone below northern Cascadia, downdip rupture propagation is not impeded unless the gap has higher dynamic friction and low shear stress rate levels. Extremely low effective normal stress in the ETS region also promotes supershear rupture, giving rise to high-frequency radiation. These results favor a deeper seismic source model for Cascadia and demonstrate that stress gradients and friction in the gap control downdip rupture extent.

Acknowledgments
This work was funded by the National Science Foundation (PREEVENTS geosciences directorate) through grant award 1663769. The data used in this study are listed in the references and supporting information. We earnestly thank an anonymous reviewer, Kim B. Olsen, and the Editor Gavin Hayes for their thoughtful comments that improved this manuscript.

References

Ampuero, J. P. (2009). SEM2DPACK: A spectral element method tool for 2D wave propagation and earthquake source dynamics, User's Guide, version 2.3.6. Retrieved from http://www.sourceforge.net/projects/sem2d/

Andrews, D. J. (1976). Rupture velocity of plain strain shear cracks. *Journal of Geophysical Research*, *81*, 5678–5689.

Andrews, D. J. (1985). Dynamic plane-strain shear rupture with a slip-weakening friction law calculated by a boundary integral method. *Bulletin of the Seismological Society of America*, *75*(1), 1–21.

Andrews, D. J. (2010). Ground motion hazard from supershear rupture. *Tectonophysics*, *493*(3–4), 216–221. https://doi.org/10.1016/j.tecto.2010.02.003

Atwater, B. F. (1987). Evidence for great Holocene earthquakes along the outer coast of Washington State. *Science*, *236*, 942–844.

Audet, P., Bostock, M. G., Christensen, N. I., & Peacock, S. M. (2009). Seismic evidence for overpressured subducted oceanic crust and megathrust fault sealing. *Nature*, *457*(7225), 76–78. https://doi.org/10.1038/nature07650

Bird, P. (2003). An updated digital model of plate boundaries. *Geochemistry, Geophysics, Geosystems*, *4*(3), 1027. https://doi.org/10.1029/2001GC000252

Bizzarri, A., & Cocco, M. (2006). A thermal pressurization model for the spontaneous dynamic rupture propagation on a three-dimensional fault: 1. Methodological approach. *Journal of Geophysical Research*, *111*, B05303. https://doi.org/10.1029/2005JB003862

Bletery, Q., Thomas, A. M., Rempel, A. W., Karlstrom, L., Sladen, A., & De Barros, L. (2016). Mega-earthquakes rupture flat megathrusts. *Science*, *354*(6315), 1027–1031. https://doi.org/10.1126/science.aag0482

Brudzinski, M. R., Schlanser, K. M., Kelly, N. J., DeMets, C., Grand, S. P., Marquez-Azua, B., & Cabral-Cano, E. (2016). Tectonic tremor and slow slip along the northwestern section of the Mexico subduction zone. *Earth and Planetary Science Letters*, *454*, 259–271. https://doi.org/10.1016/j.epsl.2016.08.004

Bruhat, L., & Segall, P. (2016). Coupling on the northern Cascadia subduction zone from geodetic measurements and physics-based models. *Journal of Geophysical Research: Solid Earth*, *121*, 8297–8314. https://doi.org/10.1002/2016JB013267

Bruhat, L., & Segall, P. (2017). Deformation rates in northern Cascadia consistent with slow updip propagation of deep interseismic creep. *Geophysical Journal International*, *211*(1), 427–449. https://doi.org/10.1093/gji/ggx317

Byerlee, J. D. (1978). Friction of rocks. *Pure and Applied Geophysics*, *116*, 615–626.

Chen, X., & McGuire, J. J. (2016). Measuring earthquake source parameters in the Mendocino triple junction region using a dense OBS array: Implications for fault strength variations. *Earth and Planetary Science Letters*, *453*, 276–287. https://doi.org/10.1016/j.epsl.2016.08.022

Das, S., & Aki, K. (1977). A numerical study of two-dimensional spontaneous rupture propagation. *Geophysical Journal of the Royal Astronomical Society*, *50*(3), 643–668. https://doi.org/10.1111/j.1365-246X.1977.tb01339.x

Day, S. M., Dalguer, L. A., Lapusta, N., & Liu, Y. (2005). Comparison of finite difference and boundary integral solutions to three-dimensional spontaneous rupture. *Journal of Geophysical Research*, *110*, B12307. https://doi.org/10.1029/2005JB003813

Delorey, A. A., Frankel, A. D., Liu, P., & Stephenson, W. J. (2014). Modeling the effects of source and path heterogeneity on ground motions of great earthquakes on the Cascadia subduction zone using 3D simulations. *Bulletin of the Seismological Society of America*, *104*(3), 1430–1446. https://doi.org/10.1785/0120130181

Dieterich, J. H. (1979). Modeling of rock friction: 1. Experimental results and constitutive equations. *Journal of Geophysical Research*, *84*, 2161–2168. https://doi.org/10.1029/JB084iB05p02161

Dunham, E. M. (2007). Conditions governing the occurrence of supershear ruptures under slip-weakening friction. *Journal of Geophysical Research*, *112*, B07302. https://doi.org/10.1029/2006JB004717

Dunham, E. M., & Archuleta, R. J. (2005). Near-source ground motion from steady state dynamic rupture pulses. *Geophysical Research Letters*, *32*, L03302. https://doi.org/10.1029/2004GL021793

Dunham, E. M., Belanger, D., Cong, L., & Kozdon, J. E. (2011). Earthquake ruptures with strongly rate-weakening friction and off-fault plasticity, Part 2: Nonplanar faults. *Bulletin of the Seismological Society of America*, *101*(5), 2308–2322. https://doi.org/10.1785/0120100076

Fang, Z., & Dunham, E. M. (2013). Additional shear resistance from fault roughness and stress levels on geometrically complex faults. *Journal of Geophysical Research: Solid Earth*, *118*, 3642–3654. https://doi.org/10.1002/jgrb.50262

Frankel, A., Wirth, E., Marafi, N., Vidale, J., & Stephenson, W. (2018). Broadband synthetic seismograms for magnitude 9 earthquakes on the Cascadia megathrust based on 3D simulations and stochastic synthetics, Part 1: Methodology and overall results. *Bulletin of the Seismological Society of America*, *108*(5A), 2347–2369. https://doi.org/10.1785/0120180034

Flueh, E. R., Fisher, M. A., Bialas, J., Childs, J. R., Klaeschen, D., Kukowski, N., et al. (1998). New seismic images of the Cascadia subduction zone from cruise SO108 — ORWELL. *Tectonophysics*, *293*, 69–94. https://doi.org/10.1016/S0040-1951(98)00091-2

Galis, M., Pelties, C., Kristek, J., Moczo, P., Ampuero, J.-P., & Mai, P. M. (2015). On the initiation of sustained slip-weakening ruptures by localized stresses. *Geophysical Journal International*, *200*(2), 890–909. https://doi.org/10.1093/gji/ggu436

Gao, H., Schmidt, D. A., & Weldon, R. J. (2012). Scaling relationships of source parameters for slow slip events. *Bulletin of the Seismological Society of America*, *102*(1), 352–360.

Gao, X., & Wang, K. (2017). Rheological separation of the megathrust seismogenic zone and episodic tremor and slip. *Nature*, *543*(7645), 416–419. https://doi.org/10.1038/nature21389

Goldfinger, C., Galer, S., Beeson, J., Hamilton, T., Black, B., Romsos, C., & Morey, A. (2017). The importance of site selection, sediment supply, and hydrodynamics: A case study of submarine paleoseismology on the northern Cascadia margin, Washington USA. *Marine Geology*, *384*, 4–46. https://doi.org/10.1016/j.margeo.2016.06.008

Goldfinger, C., Nelson, C. H., & Johnson, J. E. (2003). Holocene earthquake records from the Cascadia subduction zone and northern San Andreas fault based on precise dating of offshore turbidites. *Annual Review of Earth and Planetary Sciences*, *31*(1), 555–577. https://doi.org/10.1146/annurev.earth.31.100901.141246

Goldfinger, C., Nelson, C. H., Morey, A. E., Johnson, J. E., Patton, J. R., Karabanov, E., et al. (2012). Turbidite event history—Methods and implications for Holocene paleoseismicity of the Cascadia subduction zone: U.S. Geological Survey Professional Paper 1661–F, 170.

Goldsby, D. L., & Tullis, T. E. (2011). Flash heating leads to low frictional earthquake slip rates. *Science*, *334*, 216–218. https://doi.org/10.1126/science.1207902

Gomberg, J. (2010). Slow-slip phenomena in Cascadia from 2007 and beyond: A review. *Bulletin of the Geological Society of America*, *122*(7–8), 963–978. https://doi.org/10.1130/B30287.1

Graves, R. W., Aagaard, B. T., Hudnut, K. W., Star, L. M., Stewart, J. P., & Jordan, T. H. (2008). Broadband simulations for Mw 7.8 southern San Andreas earthquakes: Ground motion sensitivity to rupture speed. *Geophysical Research Letters*, *35*, L22302. https://doi.org/10.1029/2008GL035750

Gulick, S. P. S., Meltzer, A. M., & Clarke, S. H. (1998). Seismic structure of the southern Cascadia subduction zone and accretionary prism north of the Mendocino triple junction. *Journal of Geophysical Research*, *103*, 27,207–27,222. https://doi.org/10.1029/98JB02526

Holtkamp, S., & Brudzinski, M. R. (2010). Determination of slow slip episodes and strain accumulation along the Cascadia margin. *Journal of Geophysical Research*, *115*, B00A17. https://doi.org/10.1029/2008JB006058

Huang, Y., Ampuero, J. P., & Kanamori, H. (2014). Slip-weakening models of the 2011 Tohoku-Oki earthquake and constraints on stress drop and fracture energy. *Pure and Applied Geophysics*, *171*(10), 2555–2568. https://doi.org/10.1007/s00024-013-0718-2

Huang, Y., Meng, L., & Ampuero, J. P. (2012). A dynamic model of the frequency-dependent rupture process of the 2011 Tohoku-Oki earthquake. *Earth, Planets and Space*, *64*(12), 1061–1066. https://doi.org/10.5047/eps.2012.05.011

Ida, Y. (1972). Cohesive force across the tip of a longitudinal-shear crack and Griffith's specific surface energy. *Journal of Geophysical Research*, *77*, 3796–3805.

Kelsey, H. M., Witter, R. C., & Hemphill-Haley, E. (2002). Plate-boundary earthquakes and tsunamis of the past 5500 yr, Sixes River estuary, southern Oregon. *Geological Society of America Bulletin*, *114*, 298–314. https://doi.org/10.1130/0016-7606(2002)114<0298:PBEATO>2.0.CO;2

Kobayashi, A. (2012). Long-term slow slip event around Kochi City from 1977 to 1980 (in Japanese with English abstract). *Journal of the Seismological Society of Japan*, *64*, 63–73.

Lay, T., Kanamori, H., Ammon, C. J., Koper, K. D., Hutko, A. R., Ye, L., et al. (2012). Depth-varying rupture properties of subduction zone megathrust faults. *Journal of Geophysical Research*, *117*, B04311. https://doi.org/10.1029/2011JB009133

Leonard, L. J., Currie, C. A., Mazzotti, S., & Hyndman, R. D. (2010). Rupture area and displacement of past Cascadia great earthquakes from coastal coseismic subsidence. *Bulletin of the Geological Society of America*, *122*, 2079–2096. https://doi.org/10.1130/B30108.1

Li, D., & Liu, Y. (2016). Spatiotemporal evolution of slow slip events in a nonplanar fault model for northern Cascadia subduction zone. *Journal of Geophysical Research: Solid Earth*, *121*, 6828–6845. https://doi.org/10.1002/2016JB012857

Li, D., McGuire, J. J., Liu, Y., & Hardebeck, J. L. (2018). Stress rotation across the Cascadia megathrust requires a weak subduction plate boundary at seismogenic depths. *Earth and Planetary Science Letters*, *485*, 55–64. https://doi.org/10.1016/j.epsl.2018.01.002

Liu, Y., & Rice, J. R. (2009). Slow slip predictions based on granite and gabbro friction data compared to GPS measurements in northern Cascadia. *Journal of Geophysical Research*, *114*, B09407. https://doi.org/10.1029/2008JB00614

Lotto, G. C., Jeppson, T. N., & Dunham, E. M. (2018). Fully-coupled simulations of megathrust earthquakes and tsunamis in the Japan trench, Nankai trough, and Cascadia subduction zone. *Pure and Applied Geophysics*. https://doi.org/10.1007/s00024-018-1990-y

McCrory, P. A., Blair, J. L., Waldhauser, F., & Oppenheimer, D. H. (2012). Juan de Fuca slab geometry and its relation to Wadati-Benioff zone seismicity. *Journal of Geophysical Research*, *117*, B09306. https://doi.org/10.1029/2012JB009407

Melgar, D., LeVesque, R.-J., Dreger, D. S., & Allen, R. (2016). Kinematic rupture scenarios and synthetic displacement data: An example application to the Cascadia subduction zone. *Journal of Geophysical Research: Soild Earth*, *121*, 6658–6674. https://doi.org/10.1002/jgrb.50358.Alaska

Meng, L., Inbal, A., & Ampuero, J. P. (2011). A window into the complexity of the dynamic rupture of the 2011 Mw 9 Tohoku-Oki earthquake. *Geophysical Research Letters*, *38*, L00G07. https://doi.org/10.1029/2011GL048118

Nakata, R., Suda, N., & Tsuruoka, H. (2008). Non-volcanic tremor resulting from the combined effect of Earth tides and slow slip events. *Nature Geoscience*, *1*, 676–678. https://doi.org/10.1038/ngeo288

Nielsen, S. B. (1998). Free surface effects on the propagation of dynamic rupture. *Geophysical Research Letters*, *25*(1), 125–128. https://doi.org/10.1029/97GL03445

Olsen, K. B., Stephenson, W. J., & Geisselmeyer, A. (2008). 3D crustal structure and long-period ground motions from a M9.0 megathrust earthquake in the Pacific northwest region. *Journal of Seismology*, *12*, 145–159. https://doi.org/10.1007/s10950-007-9082

Priest, G. R., Goldfinger, C., Wang, K., Witter, R. C., Zhang, Y., & Baptista, A. M. (2010). Confidence levels for tsunami-inundation limits in northern Oregon inferred from a 10,000-year history of great earthquakes at the Cascadia subduction zone. *Natural Hazards*, *54*(1), 27–73. https://doi.org/10.1007/s11069-009-9453-5

Rice, J. R., Lapusta, N., & Ranjith, K. (2001). Rate and state dependent friction and the stability of sliding between elastically deformable solids. *Journal of the Mechanics and Physics of Solids*, *49*(9), 1865–1898. https://doi.org/10.1016/S0022-5096(01)00042-4

Rogers, G., & Dragert, H. (2003). Episodic tremor and slip on the Cascadia subduction zone: The chatter of silent slip. *Science*, *300*, 1942–1943. https://doi.org/10.1126/science.1084783

Rubinstein, J. L., Vidale, J., Gomberg, J., Bodin, P., Creager, K. C., & Malone, S. (2007). Non-volcanic tremor driven by large transient shear stresses. *Nature*, *448*, 579–582. https://doi.org/10.1038/nature06017

Satake, K., Shimazaki, K., Tsuji, Y., & Ueda, K. (1996). Time and size of a giant earthquake in Cascadia inferred from Japanese tsunami records of January 1700. *Nature*, *379*, 246–249. https://doi.org/10.1038/379246a0

Schmalzle, G. M., McCaffrey, R., & Creager, K. C. (2014). Central Cascadia subduction zone creep. *Geochemistry, Geophysics, Geosystems*, *15*, 1515–1532. https://doi.org/10.1002/2013GC00517

Scholz, C. H., & Campos, J. (2012). The seismic coupling of subduction zones revisited. *Journal of Geophysical Research*, *117*, B05310. https://doi.org/10.1029/2011JB009003

Stone, I., Vidale, J. E., Han, S., & Roland, E. (2018). Catalog of offshore seismicity in Cascadia: Insights into the regional distribution of microseismicity and its relation to subduction processes. *Journal of Geophysical Research: Solid Earth.*, *123*, 641–652. https://doi.org/10.1002/2017JB014966

Takagi, R., Obara, K., & Maeda, T. (2016). Slow slip event within a gap between tremor and locked zones in the Nankai subduction zone. *Geophysical Research Letters*, *43*, 1066–1074. https://doi.org/10.1002/2015GL066987

Tinti, S., & Armigliato, A. (2002). A 2-D hybrid technique to model the effect of topography on coseismic displacements. Application to the Umbria-Marche (central Italy) 1997 earthquake sequence. *Geophysical Journal International*, *150*(2), 542–557. https://doi.org/10.1046/j.1365-246X.2002.01721.x

Trehu, A. M., Asudeh, I., Brocher, T. M., Luetgert, J. H., Mooney, W. D., Nabelek, J. L., & Nakamura, Y. (1994). Crustal architecture of the Cascadia forearc. *Science*, *266*(5183), 237–243. https://doi.org/10.1126/science.266.5183.237

Vallée, M., Landès, M., Shapiro, N. M., & Klinger, Y. (2008). The 14 November 2001 Kokoxili (Tibet) earthquake: High-frequency seismic radiation originating from the transitions between sub-Rayleigh and supershear rupture velocity regimes. *Journal of Geophysical Research*, *113*, B07305. https://doi.org/10.1029/2007JB005520

van Rijsingen, E., Lallemand, S., Peyret, M., Arcay, D., Heuret, A., Funiciello, F., & Corbi, F. (2018). How subduction interface roughness influences the occurrence of large interplate earthquakes. *Geochemistry, Geophysics, Geosystems*, *19*, 2342–2370. https://doi.org/10.1029/2018GC007618

Wang, K., & Tréhu, A. M. (2016). Some outstanding issues in the study of great megathrust earthquakes—The Cascadia example. *Journal of Geodynamics*, *98*, 1–18. https://doi.org/10.1016/j.jog.2016.03.010

Wang, P. L., Engelhart, S. E., Wang, K., Hawkes, A. D., Horton, B. P., Nelson, A. R., & Witter, R. C. (2013). Heterogeneous rupture in the great Cascadia earthquake of 1700 inferred from coastal subsidence estimates. *Journal of Geophysical Research: Solid Earth*, *118*, 2460–2473. https://doi.org/10.1002/jgrb.50101

Wech, A. G., & Creager, K. C. (2011). A continuum of stress, strength and slip in the Cascadia subduction zone. *Nature Geoscience*, *4*(9), 624–628. https://doi.org/10.1038/ngeo1215

Williams, M. C., Tréhu, A. M., & Braunmiller, J. (2011). Seismicity at the Cascadia plate boundary beneath the Oregon continental shelf. *Bulletin of the Seismological Society of America*, *101*, 940–950. https://doi.org/10.1785/0120100198

Wirth, E., Frankel, A., Marafi, N., Vidale, J., & Stephenson, W. (2018). Broadband synthetic seismograms for magnitude 9 earthquakes on the Cascadia megathrust based on 3D simulations and stochastic synthetics, Part 2: Rupture parameters and variability. *Bulletin of the Seismological Society of America*, *108*(5A), 2370–2388. https://doi.org/10.1785/0120180029